Linear, third order nonlinear and optical limiting studies on MZO/FTO thin film system fabricated by spin coating technique for electro-optic applications

Mohd. Shkir
Advanced Functional Materials and Optoelectronics Laboratory (AFMOL), Department of Physics, College of Science, King Khalid University, Abha 61413, Saudi Arabia

Mohd. Arif
Advanced Electronic and Nanomaterials Laboratory, Department of Physics, Jamia Millia Islamia, New Delhi 110025, India

Vanga Ganesh and Mohamed A. Manthrammel
Advanced Functional Materials and Optoelectronics Laboratory (AFMOL), Department of Physics, College of Science, King Khalid University, Abha 61413, Saudi Arabia

Arun Singh
Advanced Electronic and Nanomaterials Laboratory, Department of Physics, Jamia Millia Islamia, New Delhi 110025, India

Shivaraj R. Maidur and Parutagouda Shankaragouda Patil
Department of Physics, K. L. E. Institute of Technology, Opposite Airport, Gokul, Hubballi 580030, India

Ibrahim S. Yahia, Hamed Algarni, and Salem AlFaify[a)]
Advanced Functional Materials and Optoelectronics Laboratory (AFMOL), Department of Physics, College of Science, King Khalid University, Abha 61413, Saudi Arabia

(Received 9 July 2018; accepted 9 August 2018)

Herein, we report the detailed optoelectronic characteristics of low cost fabricated pristine and 1, 5, 10, and 15 wt% Mg-doped ZnO films on the FTO substrate (MZO/FTO) through the spin coating technique. High crystallinity and single phase of the film were confirmed by X-ray diffraction investigation. The average crystallite size was in the range of 46–78 nm. Homogeneous distribution of Mg doping in ZnO was approved by elemental mapping analysis. The fiber-like surface morphology was confirmed by the scanning electron microscopy analysis. Optical transparency was observed in the range of 40–80% for the fabricated films. The optical band gaps for direct and indirect transitions obtained from Tauc's relation are in the range of 3.103–3.283 eV and 2.423–2.968 eV, respectively. It is also observed that the energy gap of MZO films decreases with an increase in Mg doping from 1 to 15%. The respective stable values of absorption and refractive indices are obtained in the range of ~0.036–0.088 and ~1.71–2.1. The linear and nonlinear optical susceptibilities as well as the nonlinear refractive index values were calculated. Additionally, Z-scan measurement was carried out at 532 nm wavelength. The nonlinear absorption coefficient and the imaginary part of third-order nonlinear susceptibility were estimated and corresponding values are obtained in the range of 0.35–123 ($\times 10^{-5}$) cm/W and 0.084–29.7 ($\times 10^{-8}$) e.s.u., respectively. Moreover, the optical limiting threshold values were obtained in the range of 2.57–6.34 kJ/cm^2. The MZO/FTO films are showing strong optical limiting behavior compared to pristine. The output results suggest that MZO films are better contenders for optoelectronic applications.

I. INTRODUCTION

Metal oxide-based nanostructured thin films have engrossed broad attention due to their exceptional properties such as large band gap, quantum confinements, high active surface area, and stability. The size and shape of nanostructures strongly influence the properties of materials.[1] Zinc oxide (ZnO) is the n-type semiconductor holding large band gap (3.37 eV) and having large free exciton binding energy 60 meV. It has found potential applications in various fields due to its high reflectivity in infrared and high transparency in visible spectrum, superior gas sensing properties, and low resistance compared to other nanostructured thin films.[2] Normally, the doping of the semiconductor with alkaline earth

[a)]Address all correspondence to this author.
e-mail: sasaalfaify@hotmail.com
DOI: 10.1557/jmr.2018.310

 © Materials Research Society 2018

https://doi.org/10.1557/jmr.2018.310 Published online by Cambridge University Press

metals such as Mg, Ca, Sr, Ba, etc. could be used to modify its structural and optical properties according to the specific requirements. The investigations on alkaline earth metal doped ZnO thin films are on achieving enhanced room temperature ferromagnetism with huge magnetic moment.[3]

Numerous reports by eminent researchers on various physical and chemical techniques are available in the literature for the growth of Mg-doped ZnO thin films, which include atomic layer deposition,[4] PLD,[5] MBE,[6] sol–gel spin coating,[7] sputtering,[8] electrochemical deposition,[9] thermal evaporator,[10] CVD,[11] spray pyrolysis,[12] etc.

Mg-doped ZnO thin films have found numerous potential applications in photovoltaic cells, gas sensors, memory devices, etc. Rod-shaped Mg-doped ZnO thin films showed gas sensing properties prepared by radio frequency sputtering technique, deposited on the sapphire substrate.[8] Spherical-shaped Mg-doped ZnO grains prepared by spray pyrolysis have reported selective gas sensing behavior to detect ammonia.[13] Amir et al. reported the very effective carbon monoxide chemical sensor-based on Mg-doped ZnO nanobelts.[14] Recently, Mg added ZnO nanocomposite films were synthesized by the PLD method, which proposed to be used as the window layer of solar cells.[15] Also, the Mg-doped ZnO interface shows excellent activity for ultraviolet exciting time resolved photoluminescence.[16] It is sound recognized that the optical band gap of a semiconductor is strongly influenced by the particle sizes where an increase in energy gap is expected with the reduction of the grain size due to quantum confinement effects. The grain size in the nanostructured thin films can be easily tuned during the synthesis process by varying the growth parameters. Accordingly, we preferred the novel sol–gel process to achieve ZnO films in the presence of Mg by the spin coating method. In recent times, this technique has been adopted for the preparation of Mg & Al co-doped ZnO films of enhanced photocurrent.[17]

In the present article, pristine ZnO and $Zn_{1-x}Mg_xO$ (x = 0.00, 0.01, 0.05, 0.10, and 0.15) nanostructured films are synthesized on FTO by the sol–gel spin coating procedure. Numerous key properties were examined such as structure by X-ray diffraction, vibrational by Raman spectroscopy, surface morphology, elemental composition, and mapping by scanning electron microscopy/energy dispersive X-ray spectroscopy (SEM/EDX), optical properties by UV-Vis-NIR spectroscopy, and nonlinear optical properties by Z-scan technique.

II. EXPERIMENTAL METHOD

The synthesis of $Zn_{1-x}Mg_xO$ (x = 0.00, 0.01, 0.05, 0.10, and 0.15) (MZO) nanostructure films was carried out using the sol–gel spin coating method on FTO substrates. Identified quantity of 0.5 M zinc acetate dihydrate (Sigma Aldrich, St. Louis, Missouri) and magnesium acetate tetrahydrate (Sigma Aldrich) have been dissolved in 20 mL 2-methoxy ethanol (Sigma Aldrich). The resultant solution was magnetically stirred for 1 h at 60 °C to acquire consistent and light-yellow color gel. Finally, 299 μmL of mono ethanolamine was added into the above prepared solutions as the stabilizer and continued the stirring at previous temperature for additional 1 h to get more inclusive fraternization of additive into the freshly prepared solution. These solutions of $Zn_{1-x}Mg_xO$ (x = 0.00, 0.01, 0.05, 0.10, and 0.15) were filtered and reserved in light-free area for 48 h to acquire gel.

Pristine and Mg-doped ZnO (MZO) nanostructure films were coated on substrates of FTO coated glass by the spin coater unit (Brewer Science, Cee, Rolla, Missouri, precision spin coaters), at ~2500 rpm for 30 s. After the deposition, films were kept on a hot plate at 120 °C for about ten minutes to eliminate the organic solvents in the deposited film, and this overall process was repeated 15 times to conquer anticipated thickness of films. Furthermore, all deposited $Zn_{1-x}Mg_xO$ (x = 1, 5, 10, and 15 wt%) films were consequently annealed at 450 °C for 2 h inside a furnace of high stability under oxygen flow.

The structural analysis of pristine/FTO and MZO/FTO films was examined by using a Shimadzu LabX XRD-6000X-ray diffractometer (Kyoto, Japan). Vibrational analysis was carried out through FT-Raman spectroscopy in the wave number range from 50 to 1500 cm^{-1} using a Thermo Scientific, DXR FTRAMAN spectrometer (Waltham, Massachusetts). The evaluation of nanostructure growth and surface morphology of prepared films was carried out using SEM (JSM 6360 LA, JEOL, Ltd., Tokyo, Japan) and AFM [NT-MDT (Type Next, Russia)] and studied grain magnitude and roughness by devoted NT-MDT software. The measurements of optical properties over a wide wavelength range, i.e., 200–1000 nm, were performed on a JASCO V-570 UV-Vis-NIR spectrophotometer. Third-order nonlinear and optical limiting investigations were performed through Z-scan measurements.

III. RESULTS AND DISCUSSION

A. Structural analysis

XRD diffractogram of pristine and MZO thin films is shown in Fig. 1(a). The respective positions of ZnO major peaks (100), (002), (001), and (110) (Zincite, JCPDS 36-1451) were observed from the recorded XRD patterns, which show that all the synthesized thin films were polycrystalline. The XRD peak (002) at 34.4° is dominant plane along with hexagonal wurtzite structure. Apart from the above observed peaks, supplementary peaks (110), (200), and (211) were observed at 2θ = 26.7°, 37°, and 52°, which correspond to the FTO substrate such as tin dioxide phase (JCPDS# 00-041-1445), the intensity of the FTO substrate peak increases with increasing Mg^{+2} doping concentrations.

https://doi.org/10.1557/jmr.2018.310 Published online by Cambridge University Press

The grain sizes for the prepared pristine/FTO and MZO/FTO films were determined form the recorded XRD patterns by applying Debye Scherer formula[18–20]: $D = \frac{k\lambda}{\beta_{2\theta}\cos\theta}$, where $\beta_{2\theta}$ is the FWHM, k is the coupling constant taken to be 0.9, λ is the wavelength used (1.5406 Å), and θ is the Bragg's angle. The calculated values of lattice parameters and crystallite size of pristine/FTO and MZO/FTO films are found to be varying with Mg concentration and are given in Table I. This difference is attributed to diversity in relative ionic size of Mg^{2+} (0.72 Å) and Zn^{2+} (0.60 Å). Moreover, the density of dislocations and microstrain were also estimated through well-known relations[21,22] and are tabulated in Table I. The highest value of D was estimated for 15% MZO, and also values of dislocation density and lattice strain are reduced, which indicates good quality of deposited films.

B. FT Raman analysis

FT-Raman spectra of pristine/FTO and MZO/FTO films are depicted in Fig. 1(b). The presence of vibrational bands at ~1095 ± 2 cm^{-1}, 950 ± 5 cm^{-1}, and 790 ± 3 cm^{-1} are might be for the substrate. The Raman peak situated at ~557 ± 3 cm^{-1} is allocated to A_1 (LO) asymmetric mode, and this might be recognized to the contributions of lower and higher wavenumbers.[23,24] However, this Raman peak is slightly shifted to the low wave number region compare to the bulk one. The Raman peak situated at ~470 ± 5 cm^{-1} (E_2 mode) is the fundamental mode of vibration for the ZnO hexagonal phase and also have shift in its position to higher wave number in contrast to films and bulk ZnO.[24,25] The possible reason behind this shift in position is the development of stress in films when deposited on the substrate, or may be due to variation in grain size due to doping. It can be visibly seen in the figure that the intensity and sharpness of Raman peaks are increased with Mg doping concentration, which indicates high crystallinity of films. All Raman peaks are found to be in well-agreement with previous reports.[26–28]

C. Microstructure and EDX analysis

Figures 2(a)–2(e) exhibit the SEM micrographs of all pristine/FTO and MZO/FTO films. SEM images showed that the whole FTO substrate is roofed by uniformly grown smaller grains, revealing the smoothness of the surface for all pure and MZO/FTO thin films. The low-magnification image clearly shows the uniformity of the

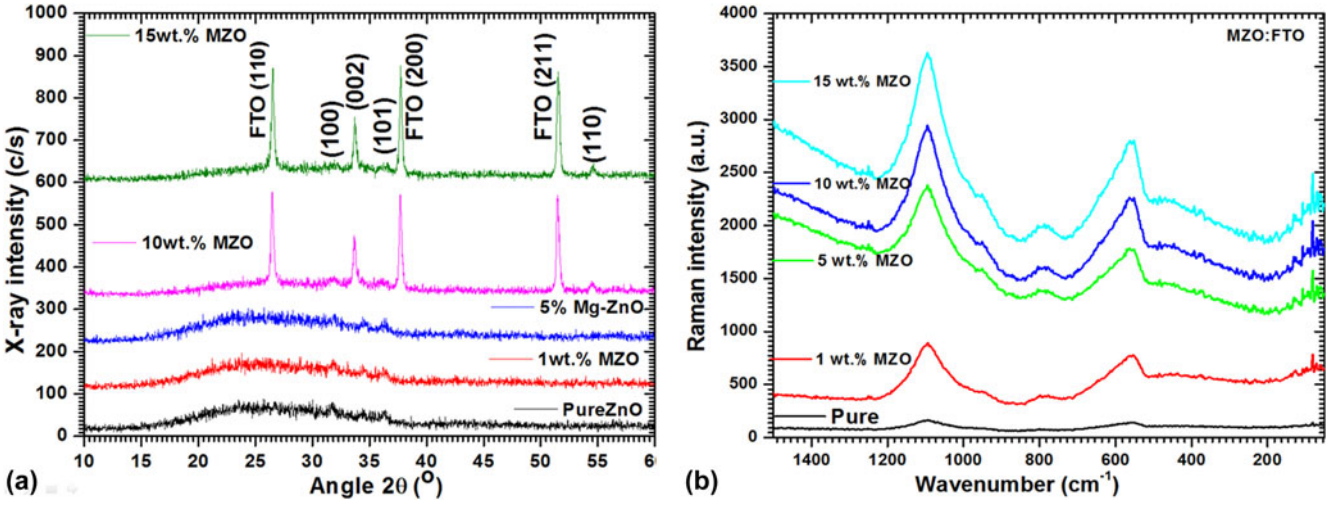


FIG. 1. (a) XRD patterns and (b) vibrational spectra for all deposited ZnO films.

TABLE I. POWDERX refined structural parameters of pristine/FTO and MZO/FTO films.

Thin films	Reported (JCPDS# 36-1451)	Pure	1% Mg	5% Mg	10% Mg	15% Mg
$a = b$ (Å)	3.2498	3.2505	3.2490	3.2422	3.2430	3.2598
c (Å)	5.2066	5.2123	5.2088	5.2170	5.2253	5.2090
V (Å)^3	...	47.69	47.62	47.49	47.59	47.94
D (nm)	...	51.318	68.742	46.597	56.920	77.578
$\delta \times 10^{-4}$	...	3.979	2.116	4.606	3.087	1.662
$\varepsilon \times 10^{-3}$	...	1.324	0.611	0.818	0.709	0.481
Mean square deviation	Before refinement	0.04008	0.07825	0.10864	0.19942	0.18789
	After refinement	0.03307	0.07881	0.07018	0.02979	0.17437

https://doi.org/10.1557/jmr.2018.310 Published online by Cambridge University Press

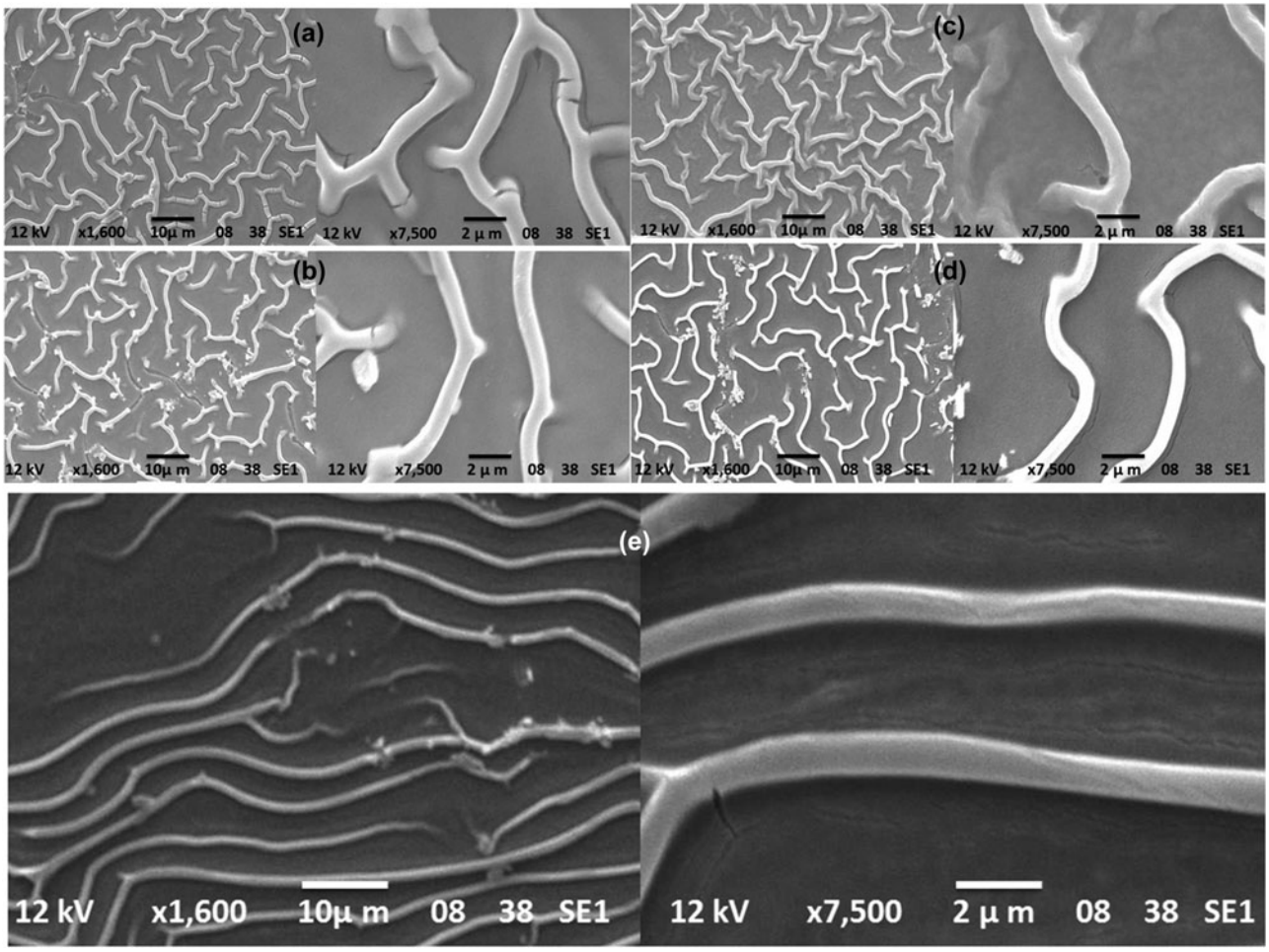


FIG. 2. SEM micrographs of (a) pristine/FTO, (b) 1%, (c) 5%, (d) 10%, and (e) 15% MZO/FTO films.

microstructure without any creaks and holes. On the other hand, at higher magnification, it can be detected that thin films are self-possessed of strongly packed and randomly arranged wire-like structures. Conferring to EDX elemental mapping results [see Fig. S1 (Supplementary Material)], magnesium is uniformly distributed over the entire surface of the prepared thin films on the FTO substrate.

D. Linear optical properties

Figures 3(a)–3(c) exhibit absorption, transmittance, and reflectance plots of pristine/FTO and MZO/FTO films. The nanostructure films hold higher transparency in the visible range. Pristine ZnO displays transmittance ~80% in the visible region, whereas this value is decreased for MZO films. Correspondingly, the absorption for pure ZnO film on FTO was found to be lower than that of MZO films. The transmittance spectra of films consist of interference fringes in the higher wavelength region, which might be due to manifold reflections at two film edges deposited on different substrates.[29] The films exhibited strong absorption in the UV, which is beneficial for various device fabrications. Analogous behaviors are detected in many metal oxide nanostructured films along with diverse dopants.[30]

Direct and indirect band gap values of pristine/FTO and MZO/FTO films were obtained through Tauc's relation[31,32]: $(\alpha h\nu)^{1/m} = A(h\nu - E_g)$, where A is the fundamental constant, h is the plank's constant, ν is the frequency, α is the absorbance coefficient, E_g is the energy gap, and m characterizes the transition process involved. Here, α was estimated from absorbance (A) and thickness (t) by equation[33] $\alpha = 2.303A/t$. The value of m equals to 2 corresponds to an allowed direct transition and 1/2 for an indirect transition.

Figures 4(a) and 4(b) represent the graphs of direct and indirect energy transitions of pristine and MZO/FTO nanostructured films. The E_g values are calculated by inducing the rectilinear area of $(\alpha h\nu)^m$ versus $h\nu$ plot. Energy gap values corresponding to both the transitions were found to be decreasing with Mg doping (5, 10, and 15%). The measured direct and indirect energy gaps are found between 3.103 and 3.283 eV for pristine and 2.423 and 2.968 eV for MZO/FTO films and are in line with earlier studies.[34–38]

https://doi.org/10.1557/jmr.2018.310 Published online by Cambridge University Press

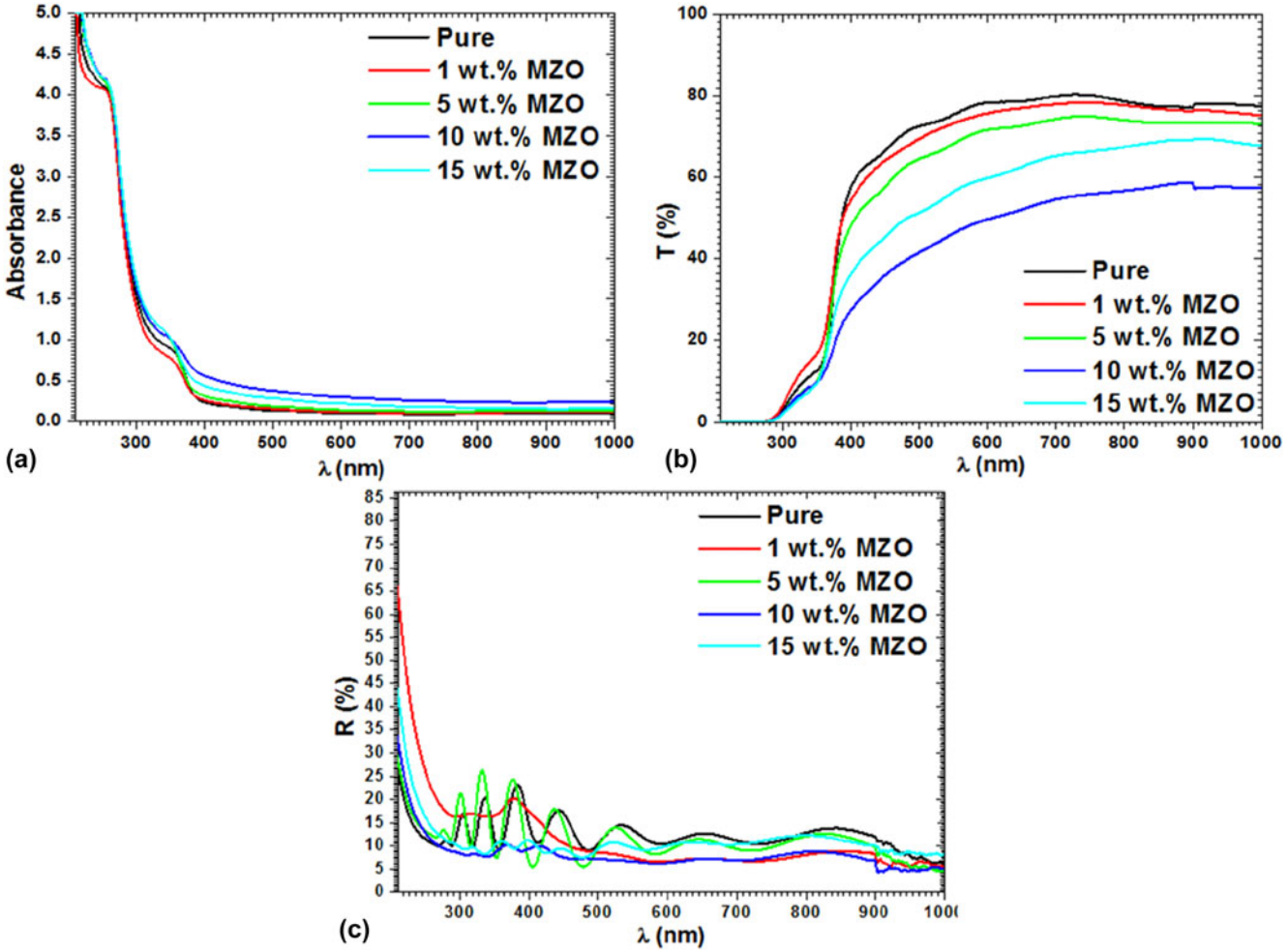


FIG. 3. (a) Absorbance, (b) transmittance, and (c) reflectance of pristine and MZO films.

Decisive optical characteristics such as index of absorption and refraction, k, and n films are work out using $k = \alpha\lambda/4\pi$ and $n = \frac{(1+R)}{(1-R)} + \sqrt{\frac{4R}{(1-R)^2} - k^2}$, where R is the function of refractive index (n) [39] and plotted in Figs. 4(c) and 4(d), respectively.

It has been observed from these plots that both n and k are displaying analogous tendency with wavelength, i.e., on increasing the wavelength, and the values of n, k are decreasing first and reach the steady state at higher wavelengths. This kind of tendency is a clear indication of defect-free growth of the synthesized nanostructure thin films. Some trivial increases in refractive index (n) are observed after 400 nm and these increases in the value of n at higher wavelengths are attributed to the consequence of magnesium doping. Moreover, similar behaviors are also reported for other metal oxide semiconductor nanostructured thin films with different dopants.[40]

In an application point of view, the variation of polarization with the energy of incident wavelength is very significant for the fabrication and optimization of an optoelectronic device. Dielectric correlated factors such as real (ε_1) and imaginary (ε_2) components of dielectric constant describe the electronic excitation spectra of any nanocrystalline films. In view of this, ε_1 and ε_2 for pristine/FTO and MZO/FTO nanostructured films are calculated by applying formulae[41,42]: $\varepsilon_1 = n^2 - k^2$ and $\varepsilon_2 = 2nk$, respectively, and depicted in Figs. S2(a) and S2(b) [see the Supplementary Material]. Through these plots, it was seen that ε_1 and ε_2 are varying from 2 to 10 and 0.1 to 0.9 in the energy range of 1.25–3.75 eV with the Mg doping, indicating the substantial influence of Mg on dielectric properties of nanostructured ZnO. These values of MZO/FTO are better than those previously reported on MZO/Glass in the mentioned energy region.[43] Fig. S2(b) [see the Supplementary Material] also denotes the dielectric loss with respect to the energy of incident photon. From the figure, the trend of dielectric loss with Mg doping in ZnO is similar to that of dielectric constant and indicates that the addition of Mg helps to reduce the defects in the film.

Figures S2(c) and S2(d) [see the Supplementary Material] display the plots for volume energy loss

https://doi.org/10.1557/jmr.2018.310 Published online by Cambridge University Press

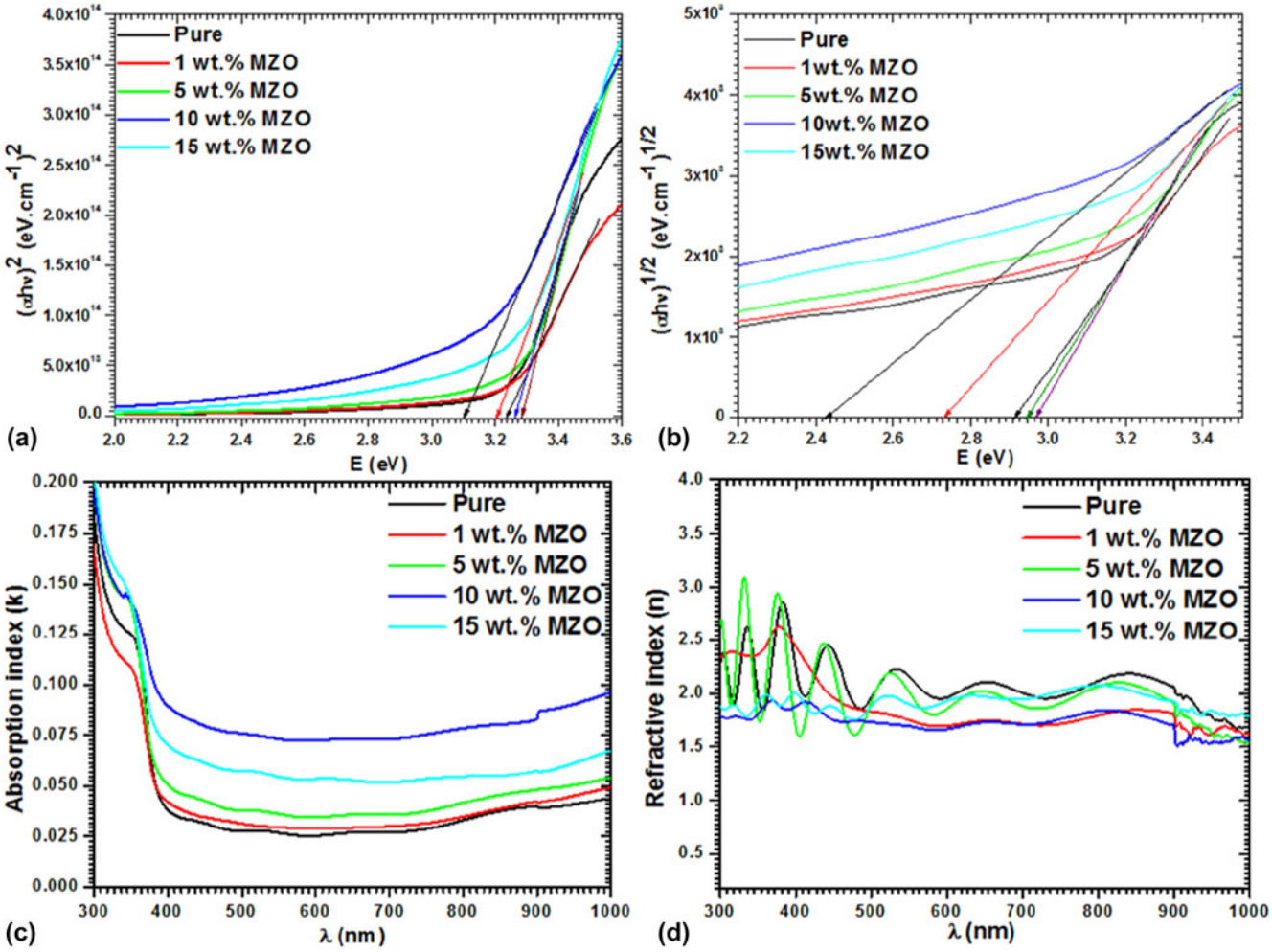


FIG. 4. (a) Direct and (b) indirect transition, (c) absorption index, and (d) refractive index of MZO/FTO films.

(VELF) and surface energy loss (SELF) functions of pristine and MZO films with respect to photon energy ($h\nu$). These are key parameters to estimate energy decay rate occurring when electrons pass over any material and are obtained from ε_1 and ε_2 using the following equation[44]:

$$\text{VELF} = -\text{Im}\left(\frac{1}{\varepsilon^*}\right) = \frac{\varepsilon_2}{\varepsilon_1^2 + \varepsilon_2^2} \text{ and SELF}$$
$$= -\text{Im}\left(\frac{1}{\varepsilon^* + 1}\right) = \frac{\varepsilon_2}{(\varepsilon_1 + 1)^2 + \varepsilon_2^2} \quad .$$

From the graphs, the VELF and SELF plots follow almost similar trend without much noteworthy differences at higher and lower energies except that the VELF values are comparatively higher than that of SELF in the entire energy level, giving a sign about the journey of radiation from inner and upper levels is the same.

E. Nonlinear studies using optical and Z-scan measurements

The inference of light rays on doped materials having high susceptibilities is very significant in several opto-electronic device applications due to the great nonlinear susceptibilities they possess, which in turn provides extensive details of the preferred sample to defy high laser beats in the course of second- and third-order effects.[39] Many research teams have been trying to apply various methodologies to assess the polarizability and refractive index and a reliable formulation is achieved as follows[30,45]: polarizability, $P = \chi^{(1)}E^{(1)} + P_{\text{NL}}$, where $P_{\text{NL}} = \chi^{(2)}E^2 + \chi^{(3)}E^3$, where $\chi^{(1)}$, $\chi^{(2)}$, & $\chi^{(3)}$ are termed as susceptibilities as linear, second-, and third-order nonlinear, respectively.

Congruently, linear refractive index $n(\lambda)$ is obtained using[46] $n(\lambda) = n_0(\lambda) + n_2(E^2)$, where n_0 and n_2 are the components of n and E^2 is the square mean of electric field, with $n_0(\lambda) \gg n_2(\lambda)$ eventually resulting in

https://doi.org/10.1557/jmr.2018.310 Published online by Cambridge University Press

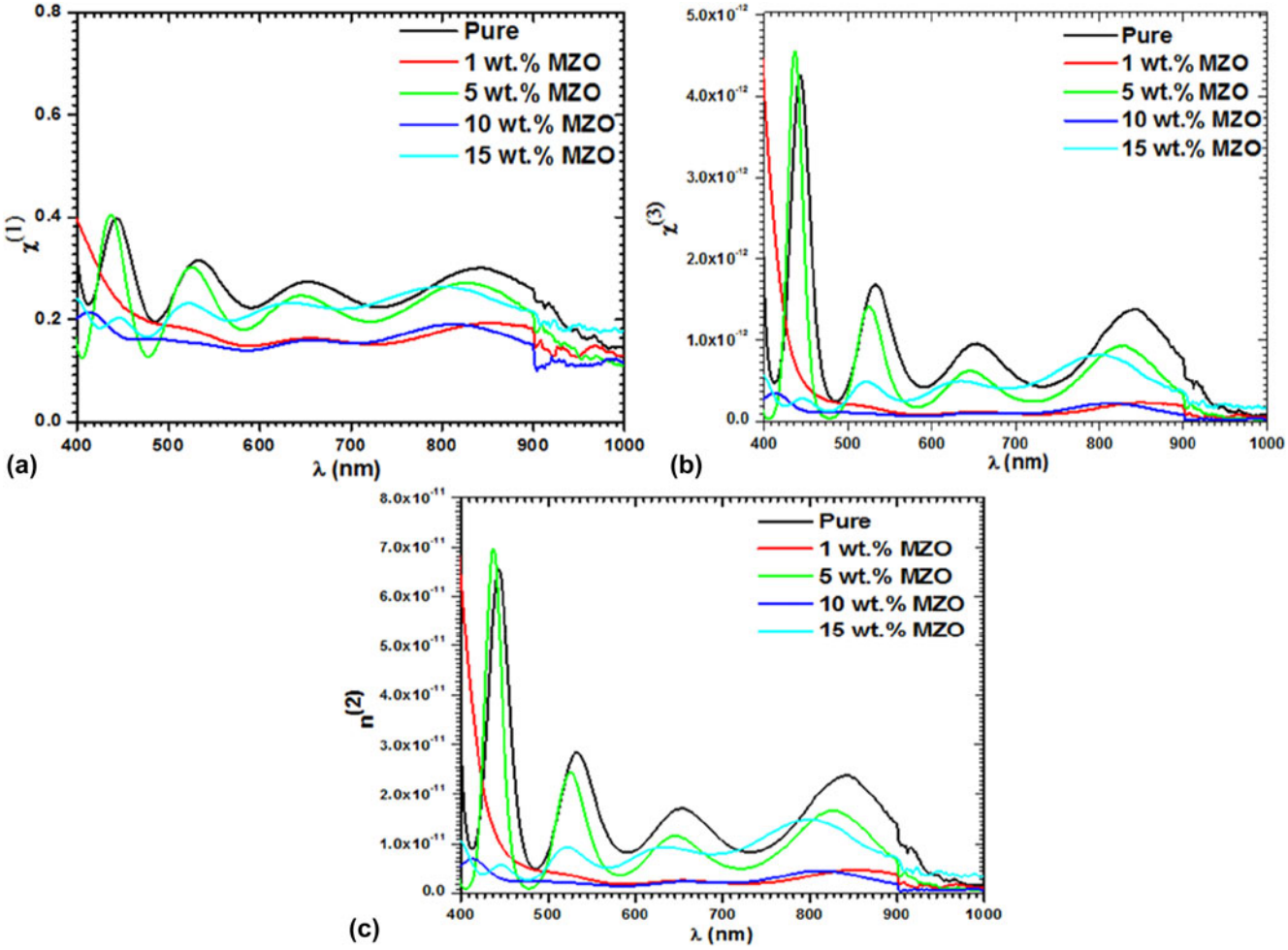


FIG. 5. (a) $\chi^{(1)}$, (b) $\chi^{(3)}$, and (c) n_2 for pristine/FTO and MZO/FTO films.

$n(\lambda) = n_0(\lambda)$. The $\chi^{(1)}$ for a given medium follows the relation[47]: $\chi^{(1)} = (n^2 - 1)/4\pi$, while the $\chi^{(3)}$ follows[42,48,49]: $\chi^{(3)} = A\chi^{(1)}$. On the other hand, $\chi^{(3)} = \frac{A}{(4\pi)^4}\left(n_0^2 - 1\right)^4$, where $A = 1.7 \times 10^{-10}$ (in e.s.u).[49] The value of n_2 is governed by[39] $n_2 = \frac{12\pi\chi^{(3)}}{n_0}$.

Figures 5(a) and 5(b) display the trends of $\chi^{(1)}$ and $\chi^{(3)}$ of the pristine/FTO as well as MZO/FTO films in terms of wavelength. From these graphs, it has been found that $\chi^{(1)}$ and $\chi^{(3)}$ values increase with growing concentration of Mg, particularly at higher wt%. This shows that doping of Mg increased the crystallinity of ZnO and also reduced the defects. At higher concentration, the overall particles' interaction with the incident photons improves and thereby improves the optical susceptibilities. The values of $\chi^{(1)}$ and $\chi^{(3)}$ are found to be from 0.1 to 0.4 and 0.023×10^{-12} to 4.59×10^{-12}, respectively, in the wavelength region 400–1000 nm. The stable values are observed compared to the previous report on MZO/glass films.[38]

Nonlinear refractive index (n_2) is also considered as a very important quantity of the material, which gives significant information regarding the capacity of the material to gather enough light when it interacts with light. Figure 5(c) represents the plot of n_2 versus wavelength for pristine/FTO and MZO/FTO thin films. The graph clearly shows an analogous trend of n_2 with $\chi^{(3)}$ and demonstrates the strong dependency of n_2 and $\chi^{(3)}$.

F. Z-scan measurement

The measured absorption of nonlinearity and limiting of optic performance of all films are demonstrated in Figs. 6(a) and 6(b). The open aperture plot displays a reverse saturation absorption process by means of a stout nonlinear absorption at the origin (focal point). This is accredited to a 2 PA nonlinear absorption procedure occurring in films. By growing the doping concentration, nonlinear absorption increased. The theoretical fitting for the experimental data was done using $T(Z) = 1 - \frac{\beta I_0 L_{\text{eff}}}{2\sqrt{2}\left(1+Z^2/Z_0^2\right)}$, where I_0 is the intensity of the CW laser at the focal Point and L_{eff} is the effective

https://doi.org/10.1557/jmr.2018.310 Published online by Cambridge University Press

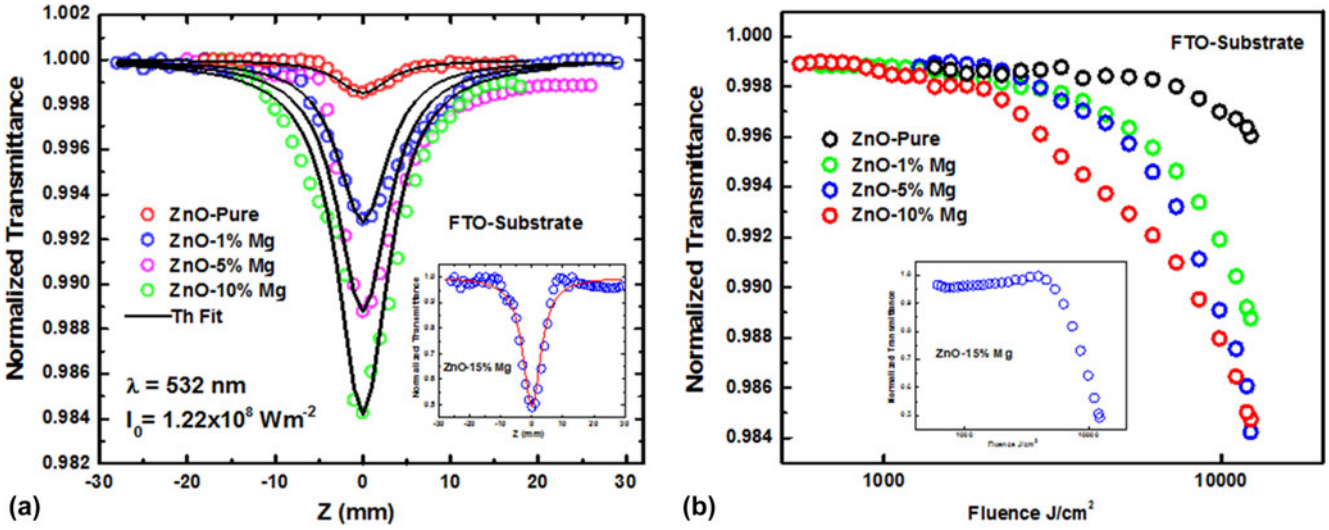


FIG. 6. Plots of Z-scan measurements for (a) absorption and (b) optical limiting.

TABLE II. Obtained NLO parameters from Z-scan study for pristine/FTO and MZO/FTO films.

Sample (FTO)	β (cm/W) × 10^{-5}	OL Th. (kJ/cm^2)	Im $\chi^{(3)}$ (e.s.u) × 10^{-8}
ZnO-pure	0.35	6.34	0.084
ZnO–1% Mg	1.7	4.51	0.41
ZnO–5% Mg	2.65	3.91	0.64
ZnO–10% Mg	3.75	3.28	0.91
ZnO–15% Mg	123	2.57	29.7

span of the material[50] used to obtain the nonlinear absorption coefficient (β). The β values are found in the range 0.35–123 ($\times 10^{-5}$) cm/W, and these values are comparatively higher than ZnO/glass films reported previously.[43]

A direct relation has been found to exist between $\chi^{(3)}$ with β and n_2 via the relation[51] $\mathrm{Im}\chi^{(3)}(\mathrm{esu}) = \frac{10^{-2}(\varepsilon_0 C^2 n_0 \beta \lambda)}{4\pi^2}\left(\frac{\mathrm{cm}^2}{\mathrm{W}}\right)$, where n_0 is the linear refractive index and C, λ, and ε_0 have their usual meaning. The calculated values of $\chi^{(3)}$ are found to be enhanced from 0.084 to 29.7 ($\times 10^{-8}$) when doped 15% Mg in ZnO. These values are comparatively higher than ZnO/glass films reported previously[43] and comparable to other reports of MZO films.[52] All these values are tabulated in Table II.

Figure 6(b) illustrates the limiting behavior of films at 532 nm DPSS CW laser. The normalized transmission is drawn against input fluence of the laser, and limiting threshold (LT) was estimated at 50% of linear transmission.[38,51] LT values were calculated to be 6.34 for pristine, 4.51, 3.91, 3.28, and 2.57 kJ/cm^2 for 1%, 5%, 10%, and 15% MZO films, respectively. The values are comparable as well higher than previous reports on MZO films.[43,52] The reduction of LT with an increase in Mg doping indicates that the MZO/FTO films are of better optical activity and could be used to shield the sensor devices from intense lights.

IV. CONCLUSIONS

Fabrication of pure and 1, 5, 10, and 15 wt% Mg-doped ZnO films of good quality is achieved through the spin coating procedure. XRD and Raman analyses approved high crystallinity and single phase of synthesized films. The variation in lattice constants was observed on doped films. Crystallite size values were obtained in the range 46–78 nm. EDX and SEM mapping studies proved that there is a homogeneous doping distribution of Mg in the ZnO matrix. The morphology of the deposited films was tested by SEM, which indicates the fiber-like structure formation. Optical absorbance, transmittance, and reflectance measurements confirm that the fabricated films possess good optical transparency, i.e., in the range of 40–80%. The calculated values of energy gaps were found in the array of 3.103–3.283 eV for direct and 2.423–2.968 eV for indirect. The optical refractive index was found in the range of ~1.71–2.1. Z-scan measurement was performed and an enhancement in the nonlinear parameter values such as β and imaginary part of $\chi^{(3)}$ are found from 0.35 to 123 ($\times 10^{-5}$) cm/W and 0.084 to 29.7 ($\times 10^{-8}$)

https://doi.org/10.1557/jmr.2018.310 Published online by Cambridge University Press

e.s.u., respectively. Optical LT values were also calculated and found to be in the range of 6.34–2.57 kJ/cm^2, indicating that MZO/FTO films show strong optical limiting behavior compared to that of pristine. The enhanced nonlinear parameters and low values of optical limiting confirm the good quality Mg-doped ZnO and may be applied in optoelectronic device fabrications.

ACKNOWLEDGMENT

The authors would like to express their gratitude to deanship of scientific research and King Khalid University, Saudi Arabia, for providing the financial support under the Project No. R.G.P. 1/54/39.

REFERENCES

1. T. Ahmad, S. Khatoon, and K. Coolahan: Structural, optical, and magnetic properties of nickel-doped tin dioxide nanoparticles synthesized by solvothermal method. *J. Am. Ceram. Soc.* **99**, 1207 (2016).
2. Ü. Özgür, Y.I. Alivov, C. Liu, A. Teke, M. Reshchikov, S. Doğan, V. Avrutin, S-J. Cho, and H. Morkoc: A comprehensive review of ZnO materials and devices. *J. Appl. Phys.* **98**, 041301 (2005).
3. S.K. Mahadeva, Z-Y. Quan, J-C. Fan, H.B. Albargi, G.A. Gehring, A.V. Riazanova, L.M. Belova, and K.V. Rao: Room temperature ferromagnetism and band gap engineering in Mg doped ZnO RF/DC sputtered films. *MRS Online Proc. Libr.* **1577**, 1 (2013).
4. Z-H. Li, E-S. Cho, and S.J. Kwon: Mg-doped ZnO thin films deposited by the atomic layer chemical vapor deposition for the buffer layer of CIGS solar cell. *Appl. Surf. Sci.* **314**, 97 (2014).
5. J.J. Park, J.K. Song, J.S. Ha, and S.M. Park: The effects of magnetic field on pulsed laser deposition of Mg-doped ZnO thin films. *Appl. Surf. Sci.* **258**, 8542 (2012).
6. W. Park, G-C. Yi, and H. Jang: Metalorganic vapor-phase epitaxial growth and photoluminescent properties of $Zn_{1-x}Mg_xO$ ($0 \le x \le 0.49$) thin films. *Appl. Phys. Lett.* **79**, 2022 (2001).
7. N.H. Hashim, S. Subramani, M. Devarajan, and A.R. Ibrahim: Properties of undoped ZnO and Mg doped ZnO thin films by sol–gel method for optoelectronic applications. *J. Aust. Ceram. Soc.* **53**, 421 (2017).
8. K. Karthick, D. Srinivasan, and J.B. Christopher: Fabrication of highly *c*-axis Mg doped ZnO on c-cut sapphire substrate by rf sputtering for hydrogen sensing. *J. Mater. Sci.: Mater. Electron.* **28**, 11979 (2017).
9. Q. Han, Y. Jeong, J. Heo, C. Shin, H. Ryu, M. Park, W. Lee, J. Yoon, J. Yang, and H. Choi: Magnesium-doped zinc oxide electrochemically grown on fluorine-doped tin oxide substrate. *J. Nanosci. Nanotechnol.* **12**, 3677 (2012).
10. Y. Zhang, J. Lu, Z. Ye, Y. Zeng, L. Zhu, and J. Huang: Quasi-aligned $Zn_{1-x}Mg_xO$ nanorods synthesized by thermal evaporation. *J. Phys. D: Appl. Phys.* **40**, 3490 (2007).
11. J. Peng, J. Guo, S. Ding, Q. Xu, H. Li, X. Tan, and X. Zhao: Mg-doped ZnO radial spherical structures via chemical vapor deposition. *Rare Met.* **30**, 292 (2011).
12. S. Kurtaran, S. Aldag, G. Ofofoglu, I. Akyuz, and F. Atay: Transparent conductive ZnO thin films grown by chemical spray pyrolysis: The effect of Mg. *J. Mater. Sci.: Mater. Electron.* **27**, 8478 (2016).
13. A.J. Kulandaisamy, J.R. Reddy, P. Srinivasan, K.J. Babu, G.K. Mani, P. Shankar, and J.B.B. Rayappan: Room temperature ammonia sensing properties of ZnO thin films grown by spray pyrolysis: Effect of Mg doping. *J. Alloys Compd.* **688**, 422 (2016).
14. M. Amin, N.A. Shah, A.S. Bhatti, and M.A. Malik: Effects of Mg doping on optical and CO gas sensing properties of sensitive ZnO nanobelts. *CrystEngComm* **16**, 6080 (2014).
15. A. Kaushal and D. Kaur: Effect of Mg content on structural, electrical and optical properties of $Zn_{1-x}Mg_xO$ nanocomposite thin films. *Sol. Energy Mater. Sol. Cells* **93**, 193 (2009).
16. S-i. Shimakawa, Y. Hashimoto, S. Hayashi, T. Satoh, and T. Negami: Annealing effects on $Zn_{1-x}Mg_xO$/CIGS interfaces characterized by ultraviolet light excited time-resolved photoluminescence. *Sol. Energy Mater. Sol. Cells* **92**, 1086 (2008).
17. A. Das, P.G. Roy, A. Dutta, S. Sen, P. Pramanik, D. Das, A. Banerjee, and A. Bhattacharyya: Mg and Al co-doping of ZnO thin films: Effect on ultraviolet photoconductivity. *Mater. Sci. Semicond. Process.* **54**, 36 (2016).
18. M. Shkir and S. AlFaify: Tailoring the structural, morphological, optical and dielectric properties of lead iodide through Nd^{3+} doping. *Sci. Rep.* **7**, 16091 (2017).
19. M. Shkir, I.S. Yahia, S. AlFaify, M.M. Abutalib, and S. Muhammad: Facile synthesis of lead iodide nanostructures by microwave irradiation technique and their structural, morphological, photoluminescence and dielectric studies. *J. Molec. Struc.* **1110**, 83 (2016).
20. M. Shkir, I.S. Yahia, V. Ganesh, H. Algarni, and S. AlFaify: Facile hydrothermal-assisted synthesis of Gd^{3+} doped PbI_2 nanostructures and their characterization. *Mater. Lett.* **176**, 135 (2016).
21. M. Shkir, M. Kilany, and I.S. Yahia: Facile microwave-assisted synthesis of tungsten-doped hydroxyapatite nanorods: A systematic structural, morphological, dielectric, radiation and microbial activity studies. *Ceram. Int.* **43**, 14923 (2017).
22. I.S. Yahia, M. Shkir, S. AlFaify, V. Ganesh, H.Y. Zahran, and M. Kilany: Facile microwave-assisted synthesis of Te-doped hydroxyapatite nanorods and nanosheets and their characterizations for bone cement applications. *Mater. Sci. Eng., C* **72**, 472 (2017).
23. C. Bundesmann, N. Ashkenov, M. Schubert, D. Spemann, T. Butz, E. Kaidashev, M. Lorenz, and M. Grundmann: Raman scattering in ZnO thin films doped with Fe, Sb, Al, Ga, and Li. *Appl. Phys. Lett.* **83**, 1974 (2003).
24. F. Decremps, J. Pellicer-Porres, A.M. Saitta, J-C. Chervin, and A. Polian: High-pressure Raman spectroscopy study of wurtzite ZnO. *Phys. Rev. B* **65**, 092101 (2002).
25. K.D.A. Kumar, S. Valanarasu, A. Kathalingam, V. Ganesh, M. Shkir, and S. AlFaify: Effect of solvents on sol–gel spin-coated nanostructured Al-doped ZnO thin films: A film for key optoelectronic applications. *Appl. Phys. A* **123**, 801 (2017).
26. X. Wei, B. Man, M. Liu, C. Xue, H. Zhuang, and C. Yang: Blue luminescent centers and microstructural evaluation by XPS and Raman in ZnO thin films annealed in vacuum, N_2 and O_2. *Phys. B* **388**, 145 (2007).
27. S.B. Yahia, L. Znaidi, A. Kanaev, and J. Petitet: Raman study of oriented ZnO thin films deposited by sol–gel method. *Spectrochimica Acta Part A: Molecular and Biomolecular Spectroscopy* **71**, 1234 (2008).
28. V. Ganesh, I.S. Yahia, S. AlFaify, and M. Shkir: Sn-doped ZnO nanocrystalline thin films with enhanced linear and nonlinear optical properties for optoelectronic applications. *J. Phys. Chem. Solids* **100**, 115 (2017).
29. J. Springer, B. Rech, W. Reetz, J. Müller, and M. Vanecek: Light trapping and optical losses in microcrystalline silicon pin solar cells deposited on surface-textured glass/ZnO substrates. *Sol. Energy Mater. Sol. Cells* **85**, 1 (2005).
30. M. Shkir, V. Ganesh, S. AlFaify, I.S. Yahia, and H.Y. Zahran: Tailoring the linear and nonlinear optical properties of NiO thin

https://doi.org/10.1557/jmr.2018.310 Published online by Cambridge University Press

films through Cr^{3+} doping. *J. Mater. Sci.: Mater. Electron.* **29**, 6446 (2018).
31. J. Tauc, R. Grigorovici, and A. Vancu: Optical properties and electronic structure of amorphous germanium. *Phys. Status Solidi B* **15**, 627 (1966).
32. M. Shakir, S. Kushwaha, K. Maurya, G. Bhagavannarayana, and M. Wahab: Characterization of ZnSe nanoparticles synthesized by microwave heating process. *Solid State Commun.* **149**, 2047 (2009).
33. M. Shkir, S. AlFaify, V. Ganesh, and I.S. Yahia: Facile one pot synthesis of PbS nanosheets and their characterization. *Solid State Sci.* **70**, 81 (2017).
34. M. Ajili, M. Castagné, and N.K. Turki: Study on the doping effect of Sn-doped ZnO thin films. *Superlattices Microstruct.* **53**, 213 (2013).
35. J. Sengupta, A. Ahmed, and R. Labar: Structural and optical properties of post annealed Mg doped ZnO thin films deposited by the sol–gel method. *Mater. Lett.* **109**, 265 (2013).
36. D. Fang, C. Li, N. Wang, P. Li, and P. Yao: Structural and optical properties of Mg-doped ZnO thin films prepared by a modified Pechini method. *Cryst. Res. Technol.* **48**, 265 (2013).
37. K. Chongsri, W. Techitdheera, and W. Pecharapa: Preparation, characterisation and photocurrent study of sol–gel-derived Al, Mg-doped ZnO transparent thin films. *Internet J. Nanotechnol.* **11**, 263 (2014).
38. M. Shkir, M. Arif, V. Ganesh, M.A. Manthrammel, A. Singh, I.S. Yahia, S.R. Maidur, P.S. Patil, and S. AlFaify: Investigation on structural, linear, nonlinear and optical limiting properties of sol–gel derived nanocrystalline Mg doped ZnO thin films for optoelectronic applications. *J. Molec. Struc.* **1173**, 375 (2018).
39. M. Shkir, V. Ganesh, S. AlFaify, and I.S. Yahia: Structural, linear and third order nonlinear optical properties of drop casting deposited high quality nanocrystalline phenol red thin films. *J. Mater. Sci.: Mater. Electron.* **28**, 10573 (2017).
40. M. Ali Omar: *Elementary Solid State Physics* (Addison-Wesley, Reading, MA, 1993).
41. A.B. Khatibani and S. Rozati: Optical and morphological investigation of aluminium and nickel oxide composite films deposited by spray pyrolysis method as a basis of solar thermal absorber. *Bull. Mater. Sci.* **38**, 319 (2015).
42. I. Yahia, V. Ganesh, M. Shkir, S. AlFaify, H. Zahran, H. Algarni, M. Abutalib, A.A. Al-Ghamdi, A. El-Naggar, and A. AlBassam: An investigation on linear and non-linear optical constants of nano-spherical CuPc thin films for optoelectronic applications. *Phys. B* **496**, 9 (2016).
43. M. Shkir, M.T. Khan, V. Ganesh, I.S. Yahia, B. Ul Haq, A. Almohammedi, P.S. Patil, S.R. Maidur, and S. AlFaify: Influence of Dy doping on key linear, nonlinear and optical limiting characteristics of SnO_2 films for optoelectronic and laser applications. *Opt. Laser Technol.* **108**, 609 (2018).
44. A. Sussman: Space-charge-limited currents in copper phthalocyanine thin films. *J. Appl. Phys.* **38**, 2738 (1967).
45. M. Frumar, J. Jedelský, B. Frumarova, T. Wagner, and M. Hrdlička: Optically and thermally induced changes of structure, linear and non-linear optical properties of chalcogenides thin films. *J. Non-Cryst. Solids* **326**, 399 (2003).
46. J. Xia, Y. Liu, X. Qiu, Y. Mao, J. He, and L. Chen: Solvothermal synthesis of nanostructured $CuInS_2$ thin films on FTO substrates and their photoelectrochemical properties. *Mater. Chem. Phys.* **136**, 823 (2012).
47. H. Ticha and L. Tichy: Semiempirical relation between non-linear susceptibility (refractive index), linear refractive index and optical gap and its application to amorphous chalcogenides. *J. Optoelectron. Adv. Mater.* **4**, 381 (2002).
48. R. Adair, L. Chase, and S.A. Payne: Nonlinear refractive index of optical crystals. *Phys. Rev. B* **39**, 3337 (1989).
49. A. Farag: Optical absorption studies of copper phthalocyanine thin films. *Opt. Laser Technol.* **39**, 728 (2007).
50. P.S. Patil, M. Shkir, S.R. Maidur, S. AlFaify, M. Arora, S.V. Rao, H. Abbas, and V. Ganesh: Key functions analysis of a novel nonlinear optical D-π-A bridge type (2*E*)-3-(4-Methylphenyl)-1-(3-nitrophenyl) prop-2-en-1-one chalcone: An experimental and theoretical approach. *Opt. Mater.* **72**, 427 (2017).
51. S.R. Maidur, P.S. Patil, S.V. Rao, M. Shkir, and S. Dharmaprakash: Experimental and computational studies on second-and third-order nonlinear optical properties of a novel d-π-a type chalcone derivative: 3-(4-methoxyphenyl)-1-(4-nitrophenyl) prop-2-en-1-one. *Opt. Laser Technol.* **97**, 219 (2017).
52. A. Agrawal, T. Ahmad Dar, R. Solanki, D.M. Phase, and P. Sen: Study of nonlinear optical properties of pure and Mg-doped ZnO films. *Phys. Status Solidi B* **252**, 1848 (2015).

Supplementary Material

To view supplementary material for this article, please visit https://doi.org/10.1557/jmr.2018.310.

https://doi.org/10.1557/jmr.2018.310 Published online by Cambridge University Press